Ab Initio Study of Polycyclic Aromatic Hydrocarbons in Their Ground and Excited States

John V. Goodpaster, James F. Harrison,* and Victoria L. McGuffin*

Department of Chemistry and Center for Fundamental Materials Research, Michigan State University, East Lansing, MI 48824-1322

Received: December 9, 1997

Both ground- and excited-state ab initio calculations are reported for four polycyclic aromatic hydrocarbons (PAHs): pyrene, benzo(*a*)pyrene, fluoranthene, and benzo(*b*)fluoranthene. Ground-state geometries, IR frequencies, excitation energies, changes in excited-state electron distributions, excited-state geometries, and excited-state frequencies are calculated and quantitatively compared to experimental data. Overall agreement with experiment is quite good, with the largest discrepancies occurring when predicting the excitation energies of the molecules. Changes in electron density correlate with changes in the excited-state geometry, with all PAHs lengthening along their axis of polarization upon excitation. These calculations are also used to examine characteristic differences between the alternant (pyrene and benzo(*a*)pyrene) and nonalternant (fluoranthene and benzo(*b*)fluoranthene) PAHs. Relative to their alternant isomers, nonalternant PAHs tend to possess higher ground-state energies, lower relative excitation energies, and greater changes in their excited-state electron densities and geometries.

I. Introduction

Polycyclic aromatic hydrocarbons (PAHs) are an important group of environmental pollutants composed solely of carbon and hydrogen, whose structures consist of two or more fused aromatic rings. These compounds are both naturally occurring and anthropogenic, and they exist at trace levels throughout the environment in a number of differing matrixes. In addition, they are the largest known class of chemical carcinogens and mutagens, with 16 PAHs identified by the U.S. Environmental Protection Agency as priority pollutants.[1] Besides their obvious environmental importance, PAHs and/or their ions are also suspected as a source of unidentified infrared emission bands (UIR bands) in the spectra of various astronomical objects.[2,3]

PAHs exist in many configurations with the number of stable isomers increasing dramatically with the number of aromatic rings. These isomers are organized into two main classes. To distinguish between them, each carbon atom in the aromatic structure is labeled, alternately skipping an atom between labels. Alternant PAHs (e.g., pyrene), have a structure such that no two atoms of the same type (labeled or unlabeled) are adjacent. Nonalternant PAHs (e.g., fluoranthene) have a structure in which such labeling results in two adjacent atoms of the same type. These structural differences can result in large changes in their chemical, spectroscopic, and toxicological properties. The differing electron distribution of the two classes of PAHs undoubtedly plays an important role in their contrasting characteristics, hence a study of the electronic structure of both alternant and nonalternant PAHs is valuable.

To date, calculations of the ground-state properties of PAHs have focused on predicting their geometries, charge distributions, ionization energies, heats of formation, and vibrational frequencies. Conjugated hydrocarbons were first treated with a self-consistent field (SCF) method by Chung and Dewar.[4] Later, other workers combined molecular mechanics and molecular orbital methods to predict the geometries and heats of formation for numerous PAHs.[5,6] Semiempirical molecular orbital calculations have also been used to compute PAH properties.[7] More recently, Schulman et al. used the Hartree−Fock (HF) method with a 6-31G* basis set to compute the geometries and heats of formation of some alternant PAHs.[8,9] The geometries of nonalternant isomers have also been calculated with both semiempirical and ab initio methods.[10] The carcinogenic activity of such isomers was estimated by computing the properties of their reactive intermediates using semiempirical methods.[11] Finally, semiempirical, ab initio, and density functional methods have been used to calculate the infrared spectra of various neutral and ionized PAHs.[12,13]

The excited-state properties of PAHs have also been studied computationally. Initial work utilized the Pariser−Parr−Pople (PPP) approximation to calculate the transition energies and intensities of alternant PAHs.[14−16] More recently, semiempirical configuration interaction (CI) methods have been used to calculate the electronic spectra of alternant and nonalternant isomers[17−19] as well as their ions and derivatives.[20,21] Furthermore, the energies of numerous PAH excited states as well as the energy gap between their highest occupied molecular orbital (HOMO) and lowest unoccupied molecular orbital (LUMO) have been predicted. The magnitude of the HOMO−LUMO energy gap was then correlated with observed photoinduced toxicity.[22] Semiempirical methods were also used by Chen and McGuffin to calculate the charge distribution of pyrene in its ground and lower excited states.[23] Both ab initio and semiempirical methods have been used to predict the absorption and emission spectra for some smaller PAHs and their radical cations.[24,25] Lastly, Gittins et al. used ab initio calculations to predict the geometry and vibrational frequencies of benzo(*a*)pyrene in its ground and excited states.[26]

Despite these advancements, ab initio calculations of large PAHs using a large basis set have been limited. Furthermore, alternant PAHs have received more attention than their nonalternant isomers, and there are few calculations involving excited states. In this work, two pairs of alternant and nonalternant

* To whom correspondence should be addressed.

S1089-5639(98)00467-8 CCC: $15.00
Published on Web 04/22/1998

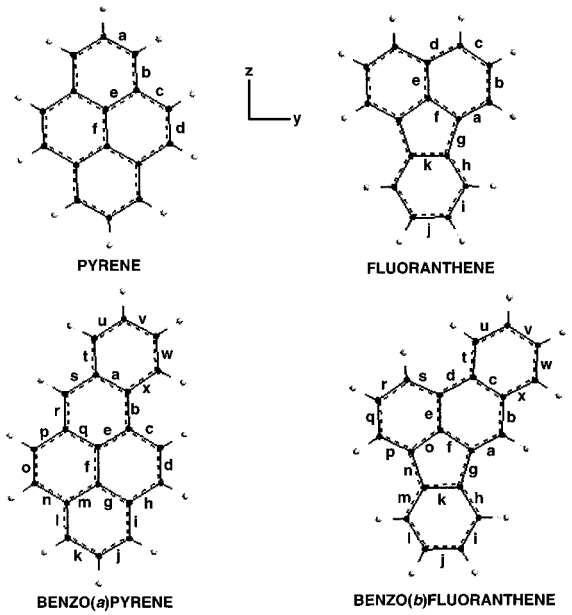

Figure 1. Optimized HF/6-31G* ground-state geometries of the four PAHs with bond and axis designations.

PAH isomers have been selected: pyrene, fluoranthene, benzo(*a*)pyrene, and benzo(*b*)fluoranthene. This set of molecules will be used to augment what is known about the properties of large PAHs in both their ground and excited states. Novel calculations reported here include the ground-state geometry of benzo(*b*)fluoranthene, the excited-state geometries of pyrene and benzo(*b*)fluoranthene, the ground- and excited-state frequencies of fluoranthene and benzo(*b*)fluoranthene, and the change in electron density for all four molecules upon excitation. Furthermore, our calculations are internally consistent, allowing direct comparison of alternant and nonalternant isomers in their ground and excited states.

II. Methods

Ground- and excited-state calculations have been completed using the Gaussian 94[27] and Spartan[28] programs on R10000 Silicon Graphics workstations. The molecular structures, together with a bond designation scheme and axis definitions, are contained in Figure 1. The PAHs were assumed to be planar with the following symmetries: pyrene (D_{2h}), fluoranthene (C_{2v}), benzo(*a*)pyrene (C_s), and benzo(*b*)fluoranthene (C_s). The optimized ground-state geometries of the four molecules were determined at the HF/6-31G* level. In order to establish that true minima had been located on the potential energy surfaces (PES), normal mode analyses of the optimized geometries were completed with a 6-31G* basis set. Finally, the electron density surfaces of the ground states were generated.

For the excited-state calculations, the Franck−Condon excitation energies for the five lowest lying singlet excited states were determined using configuration interaction with single excitations (CIS) at the optimum HF/6-31G* geometry. Selected excited-state geometries were then optimized using a 6-31G* basis set, assuming the same symmetries as above. Adiabatic transitions were calculated from the energy difference between the minima on the ground- and excited-state PES. The electron density surfaces of the excited states were also generated, and the changes in those densities from the ground state were visualized. Due to computational limitations, the frequencies of the excited states could only be determined with a 3-21G basis set (using a CIS/3-21G geometry).

III. Results and Discussion

A. Ground-State Calculations. *1. Energies and Optimized Geometries.* The optimized geometries of the four molecules together with their total energies are contained in Table 1. Our results show that the nonalternant isomers possess slightly higher calculated energies. There is a difference of 0.6 eV between pyrene and fluoranthene and a difference of 0.3 eV between benzo(*a*)pyrene and benzo(*b*)fluoranthene. These differences include the contribution from zero-point vibrational energy for each of the molecules (which was very similar between isomers). Overall these results are consistent with a greater amount of ring strain[29] and/or disrupted aromaticity[30] which is found in nonalternant molecules.

The calculated geometries for pyrene, fluoranthene, and benzo(*a*)pyrene (Table 1) agree well with published neutron diffraction results.[31−33] No experimental ground-state geometry could be found for benzo(*b*)fluoranthene, hence our results for this molecule await experimental verification. All calculated bond lengths for the PAHs fall within ±3 pm (0.03 Å) of experiment with a root mean square (rms) deviation of ±1 pm (0.01 Å). While most of the calculated values underestimate the experimental bond lengths, there are examples of the opposite. Such overestimations are uncommon, although prior calculations for pyrene,[9] fluoranthene,[10] and benzo(*a*)pyrene[26] agree with the calculated values reported here. The calculated bond angles also agree well with experiment with all deviations within ±0.3° for pyrene, ±1.5° for benzo(*a*)pyrene, and ±2.3° for fluoranthene. Finally, experimental results for the PAHs have shown that they deviate slightly from planarity in the solid state. These deviations are most likely due to thermal and/or packing forces and, hence, our assumption of planarity should not introduce significant error in calculating gas-phase properties.

The calculated SCF bond lengths for pyrene differ slightly from experiment but their relative size (c > f > e > b > a > d) is preserved. Furthermore, the calculated values tend to exaggerate differences between the bonds. Benzo(*a*)pyrene tends to have longer bond lengths in the region of the additional aromatic ring (i.e., bonds a and s), with the remainder of the molecule being similar to pyrene (i.e., bonds j and k). The bond lengths for fluoranthene are consistent with its formal structure of a benzene and naphthalene molecule joined by a long aliphatic bond. Similarly, benzo(*b*)fluoranthene resembles the joining of a benzene and phenanthrene unit.

2. Vibrational Frequencies. Ground-state vibrational frequencies of the molecules are compared with experimental spectra in Figures 2−5 and Tables IIS−VS (Supporting Information). On the basis of point groups and orientation of the PAHs, their normal modes can be assigned as follows. Pyrene in-plane vibrations have b_{1u} or b_{2u} symmetry, while out-of-plane vibrations have b_{3u} symmetry. Fluoranthene has in-plane vibrations with a_1 or b_2 symmetry and out-of-plane vibrations with a_2 or b_1 symmetry. Finally, both benzo(*a*)pyrene and benzo(*b*)fluoranthene have in-plane vibrations with a′ symmetry and out-of-plane vibrations with a″ symmetry. All calculated frequencies are scaled by a canonical factor of 0.89 to correct for electronic correlation and anharmonicity.[34] Assignment of the calculated frequencies to experimental data is based on the adjusted frequency of the normal modes, their symmetry as discussed above, and their relative intensity.

In order to quantify the extent of agreement between the calculated and experimental frequencies, the rms deviations of the predicted vibrational modes from experimental values have been calculated. These results are as follows: ±16 cm^{-1} for

TABLE l: Calculated (HF/6-31G*) versus Experimental Ground-State C−C Bond Lengths

	pyrene (D_{2h},[b] ^1A_g,[c] −611.7680[d])		fluoranthene (C_{2v},[b] $^1A_1$,[c] −611.7456[d])		benzo(*a*)pyrene (C_s,[b] $^1A'$,[c] −764.4158[d])		benzo(*b*)fluoranthene (C_s,[b] $^1A'$,[c] −764.4034[d])	
bond[a]	calcd	exptl[31]	calcd	exptl[31]	calcd	exptl[31]	calcd	exptl[31]
a	1.384	1.395	1.360	1.361	1.410	1.410	1.342	N.A.
b	1.391	1.406	1.424	1.433	1.439	1.436	1.449	N.A.
c	1.446	1.438	1.366	1.383	1.438	1.423	1.413	N.A.
d	1.339	1.367	1.423	1.415	1.345	1.352	1.459	N.A.
e	1.412	1.425	1.384	1.413	1.395	1.393	1.378	N.A.
f	1.433	1.430	1.413	1.415	1.434	1.419	1.433	N.A.
g			1.481	1.498	1.405	1.417	1.479	N.A.
h			1.379	1.390	1.432	1.441	1.380	N.A.
i			1.391	1.413	1.403	1.412	1.390	N.A.
j			1.385	1.375	1.372	1.375	1.386	N.A.
k			1.411	1.408	1.395	1.378	1.408	N.A.
l					1.380	1.402	1.390	N.A.
m					1.418	1.415	1.381	N.A.
n					1.453	1.433	1.481	N.A.
o					1.333	1.342	1.403	N.A.
p					1.453	1.446	1.368	N.A.
q					1.435	1.444	1.409	N.A.
r					1.361	1.361	1.374	N.A.
s					1.416	1.418	1.412	N.A.
t					1.421	1.425	1.406	N.A.
u					1.357	1.374	1.370	N.A.
v					1.413	1.397	1.400	N.A.
w					1.359	1.364	1.368	N.A.
x					1.422	1.418	1.407	N.A.

[a] Bond designations as shown in Figure 1; bond lengths in angstroms. [b] Symmetry. [c] State. [d] HF energy (au).

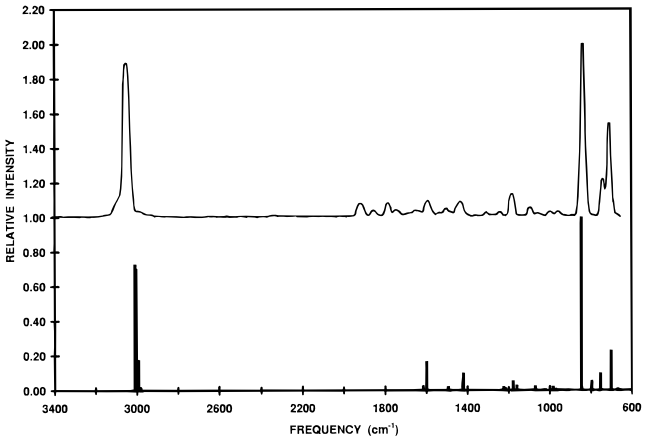

Figure 2. Experimental versus calculated (HF/6-31G*) ground-state IR frequencies for pyrene. Experimental data adapted from Semmler et al.[35]

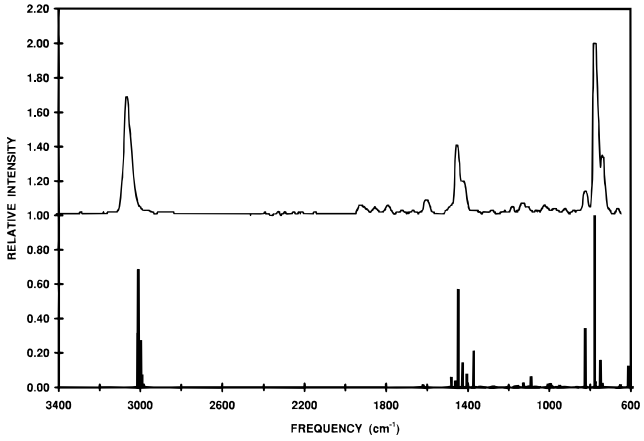

Figure 3. Experimental versus calculated (HF/6-31G*) ground-state IR frequencies for fluoranthene. Experimental data adapted from Semmler et al.[35]

pyrene (11 points), ±17 cm^{-1} for benzo(*a*)pyrene (11 points), ±22 cm^{-1} for fluoranthene (7 points), and ±27 cm^{-1} for benzo(*b*)fluoranthene (8 points). Experimental frequencies were obtained in the gas phase at 563 K and 1 atm[35] for all four PAHs with the exception of the three lowest frequency bands of pyrene, which were in the gas phase at 623 K and 1 atm.[36] For all four PAHs, deviations from experiment are the most severe when predicting the frequency of the aromatic C−H stretch. This band is found in the region 3050−3070 cm^{-1} experimentally, but was predicted to be 40−60 cm^{-1} lower in frequency. It is known from experiment that this band is sensitive to changes in both phase[35] and temperature.[13,37] While calculated frequencies correspond to gas-phase molecules, they do not account for any temperature effects.

The deviation of the calculated IR intensities from experiment has been determined using an algorithm suggested by Crawford and Morrison.[38] In this algorithm, the calculated peak intensities (P_n(calc)) and experimental peak intensities (P_n(exp)) are normalized so that their sum is unity according to the equation:

$$\sum P_n = 1 \qquad (1)$$

Then the normalized peak intensities are compared to calculate the similarity index (SI) according to the equation:

$$SI = [1 - \sum |1/2(P_n(\text{calc}) - P_n(\text{exp}))|](100\%) \qquad (2)$$

A similarity index of 100% indicates complete similarity, whereas 0% indicates complete dissimilarity. The results for the four PAHs are as follows: 87.0% for pyrene (8 points), 70.3% for benzo(*a*)pyrene (11 points), 86.6% for fluoranthene (7 points), and 69.8% for benzo(*b*)fluoranthene (8 points). This demonstrates the level of agreement obtainable when using ab initio methods to predict IR intensities. However, because of the lower agreement for benzo(*a*)pyrene and benzo(*b*)fluoranthene, the most prominent bands in the spectra are not correctly

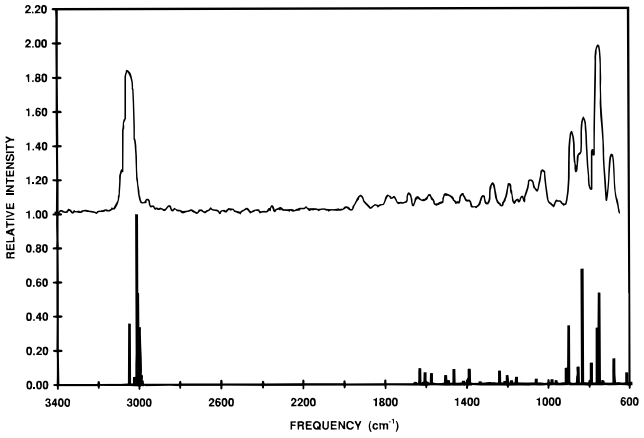

Figure 4. Experimental versus calculated (HF/6-31G*) ground-state IR frequencies for benzo(*a*)pyrene. Experimental data adapted from Semmler et al.[35]

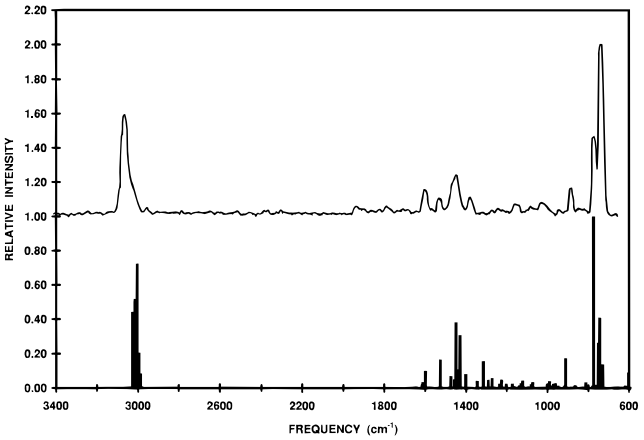

Figure 5. Experimental versus calculated (HF/6-31G*) ground-state IR frequencies for benzo(*b*)fluoranthene. Experimental data adapted from Semmler et al.[35]

identified. Theory predicts a lower intensity for the C−H bend of benzo(*a*)pyrene at 757 cm^{-1} relative to its C−H stretch as well as a lower intensity for the C−H bend of benzo(*b*)-fluoranthene at 741 cm^{-1} relative to its C−H bend at 774 cm^{-1}.

Lastly, it should be noted that our frequency assignments differ from those reported for benzo(*a*)pyrene.[26] On the basis of assignments for the other PAHs,[35] we suggest that the experimental bands in the benzo(*a*)pyrene spectrum at 757, 822, and 879 cm^{-1} are more likely out-of-plane C−H bending modes (a″ symmetry) than in-plane modes (a′ symmetry) as previously published.[26] Our calculations predict three intense modes of a″ symmetry at 752, 835, and 901 cm^{-1} which are assigned to the above experimental bands. In addition, the intensity of the calculated band at 3011 cm^{-1} implies that it, rather than the weaker calculated band at 3049 cm^{-1}, should be assigned to the most intense C−H stretching mode seen in the experimental results. Overall, these differing assignments improve the correspondence between calculation and experiment.

B. Excited-State Calculations. *1. Excitation Energies.* The calculated excitation energies for the five lowest lying singlet excited states of each PAH are contained in Table 2. There are some difficulties in comparing these results to experiment that deserve comment. First, the lack of diffuse functions in the basis set as well as no consideration of differential electron correlation contribute to an inherent overestimation of excitation energies by the CIS method. Second, the CIS method predicts gas-phase vertical excitation energies, and adiabatic energies can only be calculated when the energy of an optimized excited-state structure is also computed. The published experimental values for these compounds are exclusively adiabatic transitions, which are intrinsically lower in energy than vertical transitions. Lastly, in some cases the experimental data were acquired in the liquid or solid phase. This reduces the observed transition energies relative to the gas phase and, hence, reduces agreement with our calculations. Despite these limitations, the relative excitation energies and oscillator strengths for excited states can be reliably reproduced. What follows is a comparison of our calculated excitation energies for the four PAHs to experimental transition energies.

The excited states of pyrene have been well characterized and there is general agreement on their ordering and characteristics. The ground state of pyrene (S_0) has symmetry ^1A_g, while the lowest excited-state singlets (S_1 and S_2) have symmetry $^1B_{2u}$ and $^1B_{1u}$, respectively,[23,39] and are accessible via one-photon excitation. The $S_1 \leftarrow S_0$ transition is very weak and is polarized along the short (*y*) axis of the molecule, while the $S_2 \leftarrow S_0$ transition is much stronger and is polarized along the long (*z*) axis. In addition, the energy separation of these states is quite small (2700 cm^{-1} in the solution phase[40] or 3500 cm^{-1} in the gas phase[41]). The CIS calculations (see Table 2) correctly predict the existence of these two states, their polarizations, as well as their disproportionate oscillator strengths (0.0002 and 0.33, respectively), but invert their order. Such an inversion has been seen previously in a PPP calculation of the S_5 and S_6 states of pyrene.[16] Given the proximity of these states and the known limitations of the CIS method to estimate excitation energies, this inversion is not surprising.

The S_3 and S_4 states of pyrene are two-photon active with symmetry $^1B_{3g}$. These states have been studied using semiempirical methods,[14,15] as well as measured in a two-photon fluorescence excitation experiment of pyrene in cyclohexane.[42] In this experimental work, the authors tentatively identified another two-photon active band of ^1A_g symmetry between the S_3 and S_4 states; however, this band has not been predicted by previous calculations or by our results. Finally, the S_5 state of pyrene has $^1B_{2u}$ symmetry and is one-photon active, polarized along the short axis of the molecule. While its relative excitation energy is in agreement with experimental gas-phase results,[41] its predicted oscillator strength is significantly larger than that measured in *n*-heptane.[43]

In general, the calculated excitation energies for fluoranthene show better agreement with experiment than the results for pyrene. The ground state (S_0) has symmetry $^1A_1$ and the one-photon active S_1 through S_5 states alternate between $^1B_2$ and $^1A_1$ symmetry. The $^1B_2$ excited states are polarized along the short (*y*) axis of the molecule, while the $^1A_1$ excited states are polarized along the long (*z*) axis. Although the calculated excitation energies are higher than experiment, their relative values are correct. There are no published gas-phase excitation energies for this molecule; hence, we have compared our calculated values to experimental results acquired in 3-methylpentane at 77 K. These solid-state experimental energies are further lowered from those in the solution phase by 250−500 cm^{-1}.[44] These discrepancies notwithstanding, there is good agreement between the calculated and measured oscillator strengths. For example, the CIS model correctly predicts the forbidden nature of the first singlet. In addition, CIS calculations correctly predict lower excitation energies for fluoranthene relative to pyrene as well as a larger difference between the vertical and adiabatic excitation energies for the S_1 state. Discrepancies from experiment include the lower calculated

TABLE 2: Calculated versus Experimental Excitation Energies

	theory (CIS/6-31G*)					experiment			
molecule	state	polarization	energy (eV)[a]	energy (eV)[b]	f[c]	solvent[d]	energy (eV)[b]	f[c] or (log ϵ)[e]	ref
pyrene	$^1B_{2u}$	y	4.88	4.67	0.0002	vapor	3.41	0.002[f]	41
	$^1B_{1u}$	z	4.73	4.51	0.33	vapor	3.85	0.33[f]	41
	$^1B_{3g}$		5.81		0	CH	4.12		42
	$^1B_{3g}$		6.33		0	CH	4.29		42
	$^1B_{2u}$	y	6.60		1.06	vapor	4.68	0.35[f]	41
fluoranthene	$^1B_2$	y	4.64	4.03	0.01	3-MP	3.07	0.01	44
	$^1A_1$	z	4.88		0.39	3-MP	3.44	0.17	44
	$^1B_2$	y	5.41		0.06	3-MP	3.84	0.05	44
	$^1A_1$	z	5.85		0.14	3-MP	4.30	0.55	44
	$^1B_2$	y	6.60		0.11	3-MP	4.70	~0.14	44
benzo(*a*)pyrene	$^1A'$		4.68	4.43	0.002	HP	3.06	(3.32)[e]	46
	$^1A'$		4.33	4.04	0.43	HP	3.22	(4.47)[e]	46
	$^1A'$		5.67		0.06				
	$^1A'$		5.85		0.25	HP	4.18	(4.80)[e]	46
	$^1A'$		5.91		0.001				
benzo(*b*)fluoranthene	$^1A'$		4.75	4.18	0.08	CH	3.10	0.004	48
	$^1A'$		4.82		0.33	CH	3.36	0.50	48
	$^1A'$		5.12		0.07	CH	3.63	0.50	48
	$^1A'$		5.67		0.01	CH	4.12	0.30	48
	$^1A'$		6.03		0.71	CH	4.46	0.30	48

[a] Vertical transition. [b] Adiabatic transition. [c] Calculated and/or experimental oscillator strength. [d] CH = cyclohexane at room temperature, 3-MP = 3-methylpentane at 77 K, HP = *n*-heptane at room temperature. [e] Logarithm of the experimental molar absorptivity (L mol^{-1} cm^{-1}). [f] In *n*-heptane at room temperature (ref 43).

oscillator strength for S_4. Interestingly, this error has also been seen in previous semiempirical PPP results.[45] Lastly, the polarization of S_5 is calculated to be along the short (*y*) axis of the molecule, in contrast to experimental work where it was tentatively assigned along the long (*z*) axis.[44] However, this weak band occurs amidst stronger transitions in the fluoranthene absorbance spectrum, and its characterization must be considered incomplete.

Benzo(*a*)pyrene is similar to pyrene in that the S_1 and S_2 states are closely spaced. Furthermore, the $S_1 \leftarrow S_0$ transition is forbidden while the $S_2 \leftarrow S_0$ transition is allowed.[46,47] The calculations correctly predict these singlets, however there appears to be an inversion of the forbidden and allowed states based on their calculated oscillator strengths (see Table 2). Since the symmetry of the states is identical, their assignment is difficult. Furthermore, our calculations predict the spacing between these states to be larger than has been found in solution[46] or in the gas phase.[47] Overall agreement is somewhat improved by comparing to gas-phase results (experimental values of 3.13 eV and 3.4 eV for S_1 and S_2, respectively).[47] Of the remaining calculated singlets, only the S_4 state is assigned to an observed transition in benzo(*a*)pyrene. This assignment is based on the relative energy of the S_4 state as well as on its higher calculated oscillator strength versus the surrounding singlets. Given the forbidden nature of the calculated S_3 state, it would be difficult to discern experimentally. Note that similar oversights have occurred with the S_1 and S_3 states of fluoranthene[18] as well as the S_1 state of benzo(*b*)fluoranthene.[19]

The results for benzo(*b*)fluoranthene agree fairly well with experiment. The forbidden nature of the S_1 state is correctly predicted, although the S_1-S_2 spacing is smaller than has been found experimentally.[48] In addition, while the relative energies of the remaining singlets are correctly predicted, the calculated intensities of S_3 and S_4 are much lower than solution phase experimental data. In contrast to the trend observed for fluoranthene and pyrene, the excitation energies for benzo(*b*)-fluoranthene are higher than for its isomer benzo(*a*)pyrene, which is in agreement with experiment.[48] However, there continues to be a larger difference between the vertical and adiabatic values for benzo(*b*)fluoranthene versus benzo(*a*)-pyrene, reflecting a greater degree of relaxation in the excited state for the nonalternant PAHs.

2. Optimized Geometries. Despite the inherent overestimation of the excitation energies, it has been shown that the geometries and frequencies of excited states can be reliably simulated by using the CIS method.[26] Geometries for selected low lying singlets optimized using the CIS method are contained in Table 3. Given the close spacing of the first two excited singlets of pyrene and benzo(*a*)pyrene, both states are reported. The changes in the bond lengths from the ground state are also included in the table. All molecules have been constrained to planar geometries with the same symmetry as the ground state. Overall, the calculated bond lengths agree with semiempirical calculations for fluoranthene within ±5 pm (0.05 Å)[19] and CIS/3-21G results for benzo(*a*)pyrene within ±0.5 pm (0.005 Å).[26]

For the $^1B_{1u}$ state of pyrene, the largest changes in bond lengths occur in the central region of the molecule with a contraction along its short (*y*) axis and a lengthening along its long (*z*) axis. Bonds c and f contract by 3−4 pm, while bonds b and d lengthen by approximately the same amount. For the $^1B_{2u}$ state of pyrene, the changes in geometry yield a contraction along its long (*z*) axis and a lengthening along the short (*y*) axis. Bonds c and f contract by 3 and 6 pm, respectively, while bonds d and e lengthen by 2−3 pm.

The changes in the $^1B_2$ state of fluoranthene are even more pronounced and result in a contraction along the long (*z*) axis of the molecule, centered around the five-membered ring. The two bonds labeled g, which connect the benzene and naphthalene moieties of fluoranthene, show the largest change by contracting almost 8 pm. In contrast, bond k, which is also in the five-membered ring, lengthens by 6 pm.

Benzo(*a*)pyrene, while also an alternant PAH, shows larger changes in bond lengths than pyrene. For the S_1 ($^1A'$) state, most changes occur in alternating bonds around the perimeter of the molecule. This includes the shortening of bonds c, f, k, n, p, and x and the lengthening of bonds a, d, e, j, l, o, r, and w. In contrast, the changes in bond lengths for the S_2 ($^1A'$) state are more pronounced and clustered around the center of the molecule at bonds a, e, f, and g.

TABLE 3: Calculated (CIS/6-31G*) Excited-State C−C Bond Lengths

	pyrene (D_{2h},[b] $^1B_{2u}$,[c] −611.5962[d])		pyrene (D_{2h},[b] $^1B_{1u}$,[c] −611.6023[d])		fluoranthene (C_{2v},[b] $^1B_2$,[c] −611.5973[d])		benzo(*a*)pyrene (C_s,[b] $^1A'$,[c] −764.2528[d])		benzo(*a*)pyrene (C_s,[b] $^1A'$,[c] −764.2672[d])		benzo(*b*)fluoranthene (C_s,[b] $^1A'$,[c] −764.2496[d])	
bond[a]	calcd	change[e]	calcd	change[e]	calcd	change[e]	calcd	change[e]	calcd	change[e]	calcd	change[e]
a	1.395	0.011	1.385	0.001	1.403	0.043	1.457	0.047	1.431	0.021	1.383	0.041
b	1.398	0.006	1.419	0.028	1.386	−0.038	1.416	−0.023	1.464	0.025	1.416	−0.034
c	1.420	−0.026	1.409	−0.037	1.397	0.032	1.423	−0.014	1.409	−0.029	1.427	0.014
d	1.363	0.024	1.376	0.037	1.408	−0.015	1.363	0.018	1.365	0.021	1.453	−0.006
e	1.447	0.035	1.430	0.018	1.409	0.025	1.449	0.055	1.426	0.032	1.399	0.020
f	1.377	−0.055	1.402	−0.030	1.434	0.022	1.389	−0.045	1.408	−0.026	1.431	−0.002
g					1.404	−0.077	1.442	0.037	1.426	0.021	1.415	−0.063
h					1.418	0.039	1.416	−0.016	1.421	−0.011	1.413	0.032
i					1.355	−0.036	1.398	−0.004	1.394	−0.009	1.359	−0.031
j					1.441	0.056	1.386	0.014	1.401	0.029	1.441	0.055
k					1.473	0.062	1.396	0.001	1.369	−0.026	1.472	0.064
1							1.393	0.013	1.421	0.041	1.354	−0.035
m							1.436	0.018	1.429	0.011	1.421	0.040
n							1.427	−0.026	1.408	−0.045	1.398	−0.083
o							1.354	0.021	1.371	0.039	1.442	0.038
p							1.424	−0.029	1.413	−0.040	1.410	0.042
q							1.439	0.003	1.432	−0.003	1.372	−0.038
r							1.392	0.031	1.400	0.039	1.413	0.039
s							1.397	−0.019	1.405	−0.010	1.395	−0.018
t							1.412	−0.008	1.410	−0.010	1.412	0.006
u							1.367	0.010	1.378	0.021	1.363	−0.007
v							1.415	0.002	1.389	−0.024	1.413	0.013
w							1.366	0.007	1.392	0.033	1.358	−0.010
x							1.420	−0.002	1.389	−0.032	1.426	0.018

[a] Bond designations as shown in Figure 1; bond lengths in angstroms. [b] Symmetry. [c] State. [d] CIS energy (au). [e] Difference between excited state (CIS/6-31G*) and ground state (HF/6-31G*) optimized geometries.

Finally, in benzo(*b*)fluoranthene, as in fluoranthene, there is a large change in geometry about the five-membered ring. For example, bonds g and n contract by 6 and 8 pm, respectively, while bond k lengthens by 6 pm. Also like fluoranthene, benzo(*b*)fluoranthene demonstrates an overall contraction along the long (*z*) axis of the molecule through bonds b, i, l, and q.

It has been observed that there is a large energy loss for absorbed photons that are subsequently emitted by fluorescence of nonalternant PAHs.[49] This large Stokes shift, as well as the lack of vibrational structure in their emission spectra, has been associated with large changes in their geometry upon reaching the excited state.[49] In fact, a nonplanar excited state for fluoranthene has been proposed.[49] This possibility has been explored previously using semiempirical calculations.[19] These calculations suggested that the bond length changes for fluoranthene are large but the excited state remains planar.[19] That observation has been confirmed in this work by optimizing the geometry for fluoranthene with C_1 symmetry at the CIS/3-21G level. The deviation from planarity as measured by dihedral angles was less than ±0.02° and the bond lengths of the optimized structure were within ±0.1 pm (0.001 Å) of a constrained planar structure. Hence, it is likely that large in-plane rather than out-of-plane bond length changes are sufficient to give rise to some of the unusual excited-state properties of nonalternant PAHs.

3. Changes in Electron Density. When a molecule is promoted from the ground to excited state, the spatial distribution of electrons may undergo a significant change. These changes in electron density for the four molecules of interest are visualized in Figure 6A−F. This figure represents the subtraction of the ground-state electron density from the excited-state density, where positive differences (+0.002 electrons/a_0^3) are white and negative differences (−0.002 electrons/a_0^3) are black.

For the excited states of pyrene ($^1B_{2u}$ in Figure 6A and $^1B_{1u}$ in Figure 6B), the regions of electron density increase or decrease correspond well to bonds that shorten or lengthen, respectively, upon optimization in the excited state (Table 3). Even the relative magnitude of the change correlates with the size of the isosurface generated. In addition, the areas of electron density decrease tend to cluster along the axis of polarization (the transition moment axis) for each state. This behavior explains the overall lengthening of the molecule along its transition moment axis as described above. Finally, the transition appears to relocate electrons almost exclusively from within the π system, although the use of a smaller isovalue of ±0.001 electrons/a_0^3 is able to discern some changes in the electron density of σ bonds.

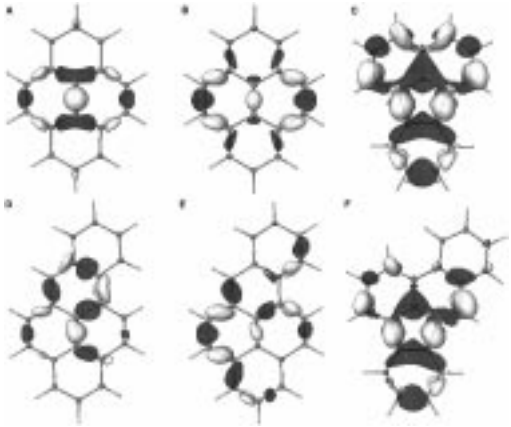

Figure 6. Visualizations of electron density differences after subtracting the ground-state electron density (HF/6-31G*) from the excited-state density (CIS/6-31G*). Positive differences (+0.002 electrons/a_0^3) are white and negative differences (−0.002 electrons/a_0^3) are black. Molecules shown are (A) pyrene ($^1B_{2u}$), (B) pyrene ($^1B_{1u}$), (C) fluoranthene ($^1B_2$), (D) benzo(*a*)pyrene (S_1, $^1A'$), (E) benzo(*a*)pyrene (S_2, $^1A'$), and (F) benzo(*b*)fluoranthene ($^1A'$).

For fluoranthene (Figure 6C), the redistribution is more complex. Around the perimeter of the molecule is an alternating pattern of electron density increase and decrease which shows good agreement with excited-state optimization results, including the large change in electron density around the central five-

TABLE 4: Excited-State Vibrations for Pyrene ($^1B_{2u}$)

symmetry	theory (CIS/3-21G) frequency (cm^{-1})	experiment (gas phase)[39,50] frequency (cm^{-1})	symmetry	theory (CIS/3-21G) frequency (cm^{-1})	experiment (gas phase)[39,50] frequency (cm^{-1})
b_{3u}	89		a_g	1017	1022
a_u	149		b_{1u}	1046	
b_{3u}	194		b_{3g}	1095	1110
b_{1g}	224		b_{2u}	1098	
b_{2g}	237		a_g	1135	1144
b_{2u}	348		b_{2u}	1146	
a_u	378		b_{3g}	1162	1155
a_g	396	393	b_{2u}	1188	
b_{3u}	448		b_{1u}	1227	
b_{3g}	450	443	a_g	1237	1250
b_{2g}	478		b_{3g}	1242	1245
b_{1u}	482		b_{2u}	1284	
b_{3g}	495	494	a_g	1288	1330
b_{1g}	498		b_{1u}	1340	
b_{2g}	508		b_{3g}	1380	1356
b_{2u}	529		a_g	1392	1424
a_g	545	572	b_{3g}	1409	1396
a_u	659		b_{2u}	1429	
b_{1u}	669		b_{1u}	1433	
b_{3u}	683		b_{3g}	1467	1466
b_{3g}	729	730	b_{2u}	1470	
b_{3u}	740		a_g	1502	1486
b_{2g}	746		b_{2u}	1525	
a_g	778	780	b_{1u}	1536	
b_{1u}	782		b_{3g}	1545	1573
b_{1g}	806		a_g	1621	1629
b_{2g}	829		b_{1u}	2978	
b_{3u}	845		b_{3g}	2978	
a_u	900		a_g	2985	
b_{2u}	912		b_{1u}	2987	
b_{1g}	916		b_{2u}	2990	
b_{1u}	951		b_{3g}	2992	
b_{2g}	967		a_g	2998	
b_{3u}	975		b_{2u}	2998	
a_u	1004		b_{1u}	3014	
b_{2g}	1008		a_g	3015	

TABLE 5: Excited-State Vibrations for Pyrene ($^1B_{1u}$)

symmetry	theory (CIS/3-21G) frequency (cm^{-1})	experiment (gas phase)[51] frequency (cm^{-1})	symmetry	theory (CIS/3-21G) frequency (cm^{-1})	experiment (gas phase)[51] frequency (cm^{-1})
b_{3u}	98		b_{2g}	1016	
a_u	142		b_{2u}	1028	
b_{3u}	200		a_g	1034	
b_{1g}	213		b_{1u}	1066	
b_{2g}	256		a_g	1119	
b_{2u}	338		b_{3g}	1123	1125
a_u	380		b_{2u}	1133	
a_g	399	412	b_{2u}	1142	
b_{3g}	437		b_{3g}	1163	
b_{2g}	473		b_{2u}	1182	
b_{3u}	479		a_g	1189	
b_{3g}	485		b_{1u}	1226	
b_{1u}	494		b_{3g}	1255	1232
b_{1g}	517		a_g	1264	
b_{2u}	526		b_{2u}	1318	
b_{2g}	550		a_g	1336	
a_g	558	600	b_{1u}	1375	
b_{1u}	663		b_{3g}	1411	1412
a_u	664		b_{2u}	1418	
b_{3u}	695		b_{1u}	1448	
b_{3g}	702		b_{3g}	1457	
b_{2g}	745		a_g	1465	
b_{3u}	753		b_{1u}	1484	
a_g	798		b_{3g}	1484	
b_{1u}	799		b_{2u}	1497	
b_{1g}	809		a_g	1502	
b_{2g}	863		b_{1u}	2980	
b_{3u}	869		b_{3g}	2981	
a_u	885		a_g	2983	
b_{1g}	906		b_{1u}	2985	
b_{2u}	919		b_{2u}	2991	
b_{1u}	955		b_{3g}	2992	
b_{3g}	979		b_{2u}	3000	
b_{2g}	988		a_g	3000	
a_u	995		b_{1u}	3008	
b_{3u}	1012		a_g	3009	

TABLE 6: Excited-State Vibrations for Benzo(*a*)pyrene ($^1A'$)

symmetry	theory (CIS/3-21G) frequency (cm^{-1})	experiment (gas phase)[26] frequency (cm^{-1})	symmetry	theory (CIS/3-21G) frequency (cm^{-1})	experiment (gas phase)[26] frequency (cm^{-1})
a″	54	54	a″	1017	
a″	75	76	a″	1019	
a″	137	141	a′	1040	1020
a″	177	175	a′	1087	
a″	199	198	a′	1093	1111
a′	208	204	a′	1129	1129
a″	267		a′	1144	
a″	276		a′	1157	
a′	326	321	a′	1172	1166
a′	370	372	a′	1180	1182
a″	379		a′	1201	1191
a″	435		a′	1216	1215
a′	450	450	a′	1236	1239
a′	474	472	a′	1260	1249
a″	481		a′	1269	1253
a″	493		a′	1278	
a′	499	515	a′	1307	
a′	508	521	a′	1332	
a″	511		a′	1339	
a″	522		a′	1365	
a′	556	551	a′	1375	
a′	590	591	a′	1412	
a′	628	625	a′	1430	
a″	660		a′	1437	
a″	676		a′	1448	
a′	676	686	a′	1463	
a″	733		a′	1485	
a′	746	748	a′	1506	
a″	753		a′	1531	
a″	756		a′	1534	
a′	780	792	a′	1537	1549
a″	811		a′	1571	
a′	818	827	a′	1618	
a″	827		a′	2977	
a″	845		a′	2980	
a″	860		a′	2983	
a′	873		a′	2983	
a″	912		a′	2986	
a″	925		a′	2991	
a′	935		a′	2994	
a′	978	960	a′	2999	
a″	986		a′	3011	
a″	991		a′	3012	
a′	999	998	a′	3020	
a″	1005		a′	3042	

membered ring. This $^1B_2$ state is polarized along the short (y) axis and, while the trend is not as clear as with pyrene, the majority of bonds that undergo a decrease in electron density and a lengthening upon excitation are oriented along this axis (i.e., bonds a, c, f, k, and j). Finally, in contrast to pyrene, it is readily apparent that electrons are redistributing between both the π and σ bonds within the molecule.

Benzo(*a*)pyrene shows results similar to those of pyrene with an alternating pattern of electron density increase and decrease around the molecule, all localized within the π system. The calculated S_1 state (Figure 6E) also shows differences from the calculated S_2 state (Figure 6D). Although the pattern of density changes are similar, they are spread more evenly throughout the molecule in the S_1 state but concentrated in the central portion of the molecule in the S_2 state. Furthermore, there are qualitative similarities between the states of benzo(*a*)pyrene and pyrene. For example, both the $^1B_{2u}$ state of pyrene and the S_2 state of benzo(*a*)pyrene have more localized changes in electron density and a larger contraction of bond f. In contrast, the $^1B_{1u}$ state of pyrene and the calculated S_1 of benzo(*a*)pyrene both possess a more uniform distribution of density changes, with a smaller contraction of the central bond f. These similarities tend to support the potential inversion of the S_1 and S_2 states of benzo(*a*)pyrene, as was seen with the $^1B_{2u}$ and $^1B_{1u}$ states of pyrene.

Finally, benzo(*b*)fluoranthene (Figure 6F) shows behavior very similar to that of fluoranthene, with a complex redistribution of electron density largely centered about the five-membered ring. In addition, exchange of density between π and σ bonds is apparent.

4. Numerical Frequencies. As mentioned above, the excited-state vibrations of the alternant and nonalternant PAHs have been calculated at the CIS/3-21G level. The effects of a smaller basis on the calculation of ground-state frequencies has been explored by Langhoff,[13] who found that increasing the size of the basis set tends to decrease the calculated frequencies and intensities only slightly. In analogous calculations for this work, increasing the basis set from 3-21G to 6-31G* for the ground state of pyrene tends to decrease those frequencies below 1400 cm^{-1} but increase those above 1400 cm^{-1}. In all cases, the change in frequency is less than 10% and there is no clear trend for changes in intensities. This suggests that the use of a smaller basis for excited-state frequencies should not introduce significant error.

TABLE 7: Excited-State Vibrations for Fluoranthene ($^1B_2$) and Benzo(*b*)fluoranthene ($^1A'$)

fluoranthene ($^1B_2$)		fluoranthene ($^1B_2$)		fluoranthene ($^1B_2$)		benzo(*b*)fluoranthene ($^1A'$)	
symmetry	frequency (cm^{-1})	symmetry	frequency (cm^{-1})	symmetry	frequency (cm^{-1})	symmetry	frequency (cm^{-1})
b_1	92	b_2	1210	a″	60	a″	1019
a_2	115	a_1	1249	a″	94	a″	1037
b_1	179	b_2	1273	a″	108	a′	1039
b_2	199	a_1	1293	a″	143	a″	1040
a_2	218	a_1	1299	a′	157	a′	1060
b_1	276	b_2	1306	a″	230	a′	1079
a_1	343	a_1	1344	a″	251	a′	1115
a_2	379	b_2	1364	a′	260	a′	1119
b_2	407	b_2	1426	a″	298	a′	1159
b_1	436	a_1	1427	a′	313	a′	1173
a_1	476	a_1	1443	a′	374	a′	1182
b_1	500	a_1	1448	a″	395	a′	1188
a_2	514	b_2	1468	a″	422	a′	1214
a_1	539	a_1	1504	a′	451	a′	1245
b_2	557	a_1	1520	a″	469	a′	1256
b_1	576	b_2	1521	a″	504	a′	1259
b_2	606	b_2	1557	a″	528	a′	1277
a_2	617	b_2	2981	a′	537	a′	1303
a_1	638	a_1	2982	a′	554	a′	1304
b_2	732	b_2	2992	a″	581	a′	1341
a_2	733	a_1	2998	a′	587	a′	1358
b_1	764	b_2	2999	a″	598	a′	1383
b_1	768	a_1	3001	a′	604	a′	1414
a_1	768	b_2	3010	a′	644	a′	1431
a_2	786	b_2	3013	a′	661	a′	1438
a_1	834	a_1	3013	a″	745	a′	1449
b_1	844	a_1	3019	a′	746	a′	1463
a_2	865			a″	753	a′	1481
a_2	880			a″	758	a′	1506
b_1	903			a′	763	a′	1520
a_1	919			a″	773	a′	1532
b_2	953			a″	782	a′	1552
b_2	973			a″	836	a′	1587
a_2	1013			a″	845	a′	2979
b_1	1013			a′	857	a′	2988
b_1	1017			a′	858	a′	2991
a_1	1030			a″	877	a′	2992
a_2	1039			a″	900	a′	2998
a_1	1056			a″	911	a′	2999
b_2	1056			a′	919	a′	3002
b_2	1063			a′	926	a′	3009
b_2	1124			a′	986	a′	3011
a_1	1164			a″	1005	a′	3014
b_2	1180			a″	1011	a′	3020
a_1	1188			a′	1017	a′	3023

The CIS/3-21G results for the $^1B_{2u}$ and $^1B_{1u}$ states of pyrene are reported in Tables 4 and 5 and compared with experimental results using supersonic jet expansions. In the fluorescence excitation experiments, only vibrational modes of a_g or b_{3g} symmetry are observed. For both excited states, modes with a_g symmetry arise from Franck−Condon overlap with the ground state, while b_{3g} modes tend to arise from vibronic coupling of the excited states.[50] Overall, the agreement of the calculated frequencies of the $^1B_{2u}$ state of pyrene with supersonic expansion results[39,50,51] is satisfactory with an rms deviation of ± 17 cm^{-1} (20 points), which is larger than that of the ground state but still quite good. In this case, assignment of vibrational modes above 1700 cm^{-1} is difficult due to the presence of many combination and overtone bands from lower energy modes, as well as the overlapping transitions from the $^1B_{1u}$ state which complicate the experimental spectra.[50]

Vibrations of the $^1B_{1u}$ state of pyrene have also been observed experimentally.[39,51] Although no experimental symmetry designations have been reported, some tentative assignments are made in Table 5. The rms deviation from experiment is larger than the $^1B_{2u}$ state at ± 22 cm^{-1} (5 points), but this is to be expected given the difficulty of resolving these bands experimentally.

The excited state vibrations for benzo(*a*)pyrene are contained in Table 6. Both the number and range of frequencies are larger than for pyrene. Gittins et al. compared the calculated frequencies for the S_1 state of benzo(*a*)pyrene to those obtained for the experimental S_1 state and found good agreement with an rms deviation of only ± 5 cm^{-1} (32 points).[26] However, on the basis of our calculated oscillator strengths of the first two states of benzo(*a*)pyrene and their similar excitation character when compared to the $^1B_{2u}$ and $^1B_{1u}$ states of pyrene (Figure 6), we suspect that an inversion of states has occurred in the calculations for this molecule. Hence, the experimental frequencies should be compared to those calculated for the higher singlet state. This comparison results in slightly poorer agreement, with an rms deviation of ± 9 cm^{-1} (32 points).

Lastly, the calculated frequencies for the excited states of fluoranthene and benzo(*b*)fluoranthene are included in Table 7. The increase in the number and range of frequencies with the size of the PAH can also been seen in these nonalternant

compounds. However, no experimental results for the excited state frequencies of the nonalternant PAHs could be found for comparison.

IV. Summary

Ground-state geometries are reliably predicted by the ab initio method and agree well with experimental crystallographic results. In addition, the total energies of the PAHs reflect the greater stability of the alternant isomers. The calculations reliably predict the ground-state IR spectra in good agreement with gas-phase experimental results, with the greatest discrepancies occurring when predicting the frequency of the C−H stretching vibration.

The prediction of either vertical or adiabatic excitation energies is not as accurate, given the inherent overestimation of the CIS method. However, the relative excitation energies and intensities are more reliably calculated. Interestingly, it appears that, in the case of the alternant isomers, the CIS method with a 6-31G* basis set has inverted the two lowest lying singlet states. Despite these limitations, the changes in the electron density of the molecules agree well with calculated excited-state geometries, and reveal a lengthening of the molecules along their axis of polarization. In addition, the nonalternant isomers dramatically contract along the long aliphatic bonds within their five-membered rings upon excitation. Finally, the excited-state frequencies for the alternant isomers compare well to gas-phase fluorescence excitation results. Overall, the ab initio methods presented here have provided a deeper insight into the ground- and excited-state properties of four environmentally and astronomically relevant compounds, as well as expanding what is known about alternant and nonalternant PAHs.

Acknowledgment. This material is based upon work supported under a National Science Foundation Graduate Fellowship to J.V.G. The authors would also like to acknowledge computing resources provided by the National Science Foundation under instrument grant CHE9321436 and computing time provided by the National Partnership for Advanced Computational Infrastructure. Additional support was provided by the U.S. Department of Energy, Office of Basic Energy Sciences, under Grant DE-FG02-89ER14056 and the MSU Center for Fundamental Materials Research.

Supporting Information Available: Cartesian coordinates for all optimized ground- and excited-state geometries (Table IS). Calculated ground-state frequencies, intensities, and symmetries for the four PAHs with comparisons to experimental data (Tables IIS−VS). (10 pages). Ordering information is given on any current masthead page.

References and Notes

(1) Lee, M. L.; Novotny, M. V.; Bartle, K. D. *Analytical Chemistry of Polycyclic Aromatic Compounds*; Academic Press: New York, 1981.
(2) Leger, A.; Puget, J. L. *Astron. Astrophys.* **1984**, *137*, L5.
(3) Allamandola, L. J.; Tielens, A. G.; Baker, J. R. *Astrophys. J.* **1985**, *290*, L25.
(4) Chung, A. H.; Dewar, M. S. *J. Chem. Phys.* **1965**, *42*, 756.
(5) Kao, J.; Allinger, N. L. *J. Am. Chem. Soc.* **1977**, *99*, 975.
(6) Kao, J. *J. Am. Chem. Soc.* **1987**, *109*, 3817.
(7) Hites, R. A.; Simonsick, W. J. *Calculated Molecular Properies of Polycyclic Aromatic Hydrocarbons*; Elsevier: Amsterdam, 1987.
(8) Schulman, J. M.; Peck, R. C.; Disch, R. L. *J. Am. Chem. Soc.* **1989**, *111*, 5675.
(9) Peck, R. C.; Schulman, J. M.; Disch, R. L. *J. Phys. Chem.* **1990**, *94*, 6637.
(10) Plummer, B. F.; Steffen, L. K.; Herndon, W. C. *Struct. Chem.* **1993**, *4*, 279.
(11) Rabinowitz, J. R.; Little, S. B. *Int. J. Quantum Chem.* **1994**, *52*, 681.
(12) Vala, M.; Szczepanski, J.; Pauzat, F.; Parisel, O.; Talbi, D.; Ellinger, Y. *J. Phys. Chem.* **1994**, *98*, 9187.
(13) Langhoff, S. R. *J. Phys. Chem.* **1996**, *100*, 2819.
(14) Nishimoto, K.; Forster, L. S. *Theor. Chim. Acta (Berlin)* **1965**, *3*, 407.
(15) Nishimoto, K. *Theor. Chim. Acta (Berlin)* **1967**, *7*, 207.
(16) Pucci, R.; Baldo, M.; Martin-Rodero, A.; Piccitto, G.; Tomasello, P. *Int. J. Quantum Chem.* **1984**, *26*, 783.
(17) Das Gupta, N. K.; Birss, F. W. *Bull. Chem. Soc. Jpn.* **1978**, *51*, 1211.
(18) Das Gupta, A.; Chatterjee, S.; Das Gupta, N. K. *Bull. Chem. Soc. Jpn.* **1979**, *52*, 3070.
(19) Suhnel, J.; Kempka, U.; Gustav, K. *J. F. Prakt. Chem.* **1980**, *322*, 649.
(20) Du, P.; Salama, F.; Loew, G. H. *Chem. Phys.* **1993**, *173*, 421.
(21) Negri, F.; Zgierski, Z. *J. Chem. Phys.* **1994**, *100*, 1387.
(22) Mekenyan, O. G.; Ankley, G. T.; Veith, G. D.; Call, D. J. *SAR and QSAR in Environmental Research* **1994**, *2*, 237.
(23) Chen, S. H.; McGuffin, V. L. *Appl. Spectrosc.* **1994**, *48*, 596.
(24) Niederalt, C.; Grimme, S.; Peyerimhoff, S. D. *Chem. Phys. Lett.* **1995**, *245*, 455.
(25) Negri, F.; Zgierski, M. Z. *J. Chem. Phys.* **1996**, *104*, 3486.
(26) Gittins, C. M.; Rohlfing, E. A.; Rohlfing, C. M. *J. Chem. Phys.* **1996**, *105*, 7323.
(27) Frisch, M. J.; Trucks, G. W.; Schlegel, H. B.; Gill, P. M. W.; Johnson, B. G.; Robb, M. A.; Cheeseman, J. R.; Keith, T.; Petersson, G. A.; Montgomery, J. A.; Raghavachari, K.; Al-Laham, M. A.; Zakrzewski, V. G.; Ortiz, J. V.; Foresman, J. B.; Cioslowski, J.; Stefanov, B. B.; Nanayakkara, A.; Challacombe, M.; Peng, C. Y.; Ayala, P. Y.; Chen, W.; Wong, M. W.; Andres, J. L.; Replogle, E. S.; Gomperts, R.; Martin, R. L.; Fox, D. J.; Binkley, J. S.; Defrees, D. J.; Baker, J.; Stewart, J. P.; Head-Gordon, M.; Gonzalez, C.; Pople, J. A. *Gaussian 94*, Revision D.3; Gaussian, Inc.: Pittsburgh, 1995.
(28) Spartan, Version 3.1; Wavefunction, Inc.: Irvine, CA, 1994.
(29) Blumer, M. *Sci. Am.* **1976**, *234*, 35.
(30) Yates, K. *Huckel Molecular Orbital Theory*; Academic Press: New York, 1978.
(31) Hazell, A. C.; Larson, F. K.; Lehmann, M. S. *Acta Crystallogr.* **1972**, *B28*, 2977.
(32) Hazell, A. C.; Jones, D. W.; Sowden, J. M. *Acta Crystallogr.* **1977**, *B33*, 1516.
(33) Iball, J.; Scrimgeour, S. N.; Young, D. W. *Acta Crystallogr.* **1976**, *B32*, 328.
(34) Hehre, W. J.; Radom, L.; Schleyer, P. R.; Pople, J. A. *Ab Initio Molecular Orbital Theory*; Wiley: New York, 1986.
(35) Semmler, J.; Yang, P. W.; Crawford, G. E. *Vib. Spectrosc.* **1991**, *2*, 189.
(36) Zhang, K.; Guo, B.; Colarusso, P.; Bernath, P. F. *Science* **1996**, *274*, 582.
(37) Pouchert, C. *The Aldrich Library of FTIR Spectra Volume 3: Vapor Phase*, 1st ed.; Aldrich Chemical Company, Inc.: Milwaukee, 1989.
(38) Crawford, L. R.; Morrison, J. D. *Anal. Chem.* **1968**, *40*, 1464.
(39) Ohta, N.; Baba, H.; Marconi, G. *Chem. Phys. Lett.* **1987**, *133*, 222.
(40) Marconi, G.; Salvi, P. R. *Chem. Phys. Lett.* **1986**, *123*, 254.
(41) Becker, R. S.; Singh, I. S.; Jackson, E. A. *J. Chem. Phys.* **1963**, *38*, 2144.
(42) Salvi, P. R.; Foggi, P.; Castellucci, E. *Chem. Phys. Lett.* **1983**, *98*, 206.
(43) Tanaka, J. *Bull. Chem. Soc. Jpn.* **1964**, *38*, 86.
(44) Kolc, J.; Thulstrup, E. W.; Michl, J. *J. Am. Chem. Soc.* **1974**, *96*, 7188.
(45) Michl, J. *J. Mol. Spectrosc.* **1969**, *30*, 66.
(46) Malkin, J. *Photophysical and Photochemical Properties of Aromatic Compounds*; CRC Press: Ann Arbor, 1992; p 92.
(47) Greenblatt, G. D.; Nissani, E.; Zaroura, E.; Haas, Y. *J. Phys. Chem.* **1987**, *91*, 570.
(48) Souto, M. A.; Otteson, D.; Michl, J. *J. Am. Chem. Soc.* **1978**, *100*, 6892.
(49) Berlman, I. B. *J. Phys. Chem.* **1970**, *74*, 3085.
(50) Borisevich, N. A.; Vodovatov, L. B.; D'yachenko, G. G.; Petukhov, V. A.; Semyonov, M. A. *J. Appl. Spectrosc.* **1995**, *62*, 482.
(51) Mangle, E. A.; Topp, M. R. *J. Phys. Chem.* **1986**, *90*, 802.